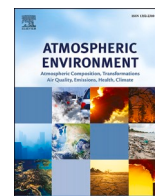




Contents lists available at ScienceDirect

Atmospheric Environment

journal homepage: www.elsevier.com/locate/atmosenv

Overview of the performance of satellite fire products in China: Uncertainties and challenges

Jinxi Chen^a, Rong Li^b, Minghui Tao^{a,*}, Lili Wang^c, Changqing Lin^d, Jun Wang^e, Lunche Wang^a, Yi Wang^a, Liangfu Chen^f

^a Key Laboratory of Regional Ecology and Environmental Change, School of Geography and Information Engineering, China University of Geosciences, Wuhan, 430074, China

^b School of Resources and Environmental Science, Hubei University, Wuhan, 430062, China

^c State Key Laboratory of Atmospheric Boundary Layer Physics and Atmospheric Chemistry, Institute of Atmospheric Physics, Chinese Academy of Sciences, Beijing, 100029, China

^d Division of Environment and Sustainability, The Hong Kong University of Science and Technology, Hong Kong, 999077, China

^e Center for Global and Regional Environmental Research, The University of Iowa, Iowa City, IA, 52242, USA

^f State Key Laboratory of Remote Sensing Science, Aerospace Information Research Institute, Chinese Academy of Sciences, Beijing, 100101, China

HIGHLIGHTS

- We evaluate the general performance of the common satellite fire products in eastern China.
- Both polar-orbiting and geostationary satellite observations have large omission ratios for the agricultural fires.
- UVA supervisions reveal prevalent small agricultural fires not detected in the common satellite detection.

ARTICLE INFO

Keywords:

Biomass burning
Satellite
Fire detection
Evaluation
Eastern China

ABSTRACT

Satellite fire observations provide an essential constraint for the estimation of global biomass burning emissions. In this study, we present a comprehensive insight into the performance of the common satellite fire products in eastern China. Despite consistent spatial patterns, both polar-orbiting and geostationary satellite observations have large omission errors for the agricultural burning fires. Owing to a coarse resolution of 2 km, approximately 90% of the concurrent 375 m Visible infrared Imaging Radiometer (VIIRS) fires are not detected in Himawari-8 products. Nevertheless, the total amount of daily Himawari-8 fires is much higher than those of VIIRS and 1 km Moderate resolution imaging spectroradiometer (MODIS). The peak time of diurnal fire counts in eastern China has obvious seasonal variations, some of which are missed by polar-orbiting satellite detection. Validation by 3 m PlanetScope images shows that VIIRS and MODIS have a very high accuracy in detecting crop straw burning fires. However, Himawari-8 fires have obvious false alarms due largely to their algorithm defects. Also, the coarse resolution of Himawari-8 tends to make fire detection more likely to be obscured by dense smoke. The unmanned aerial vehicle (UAV) supervisions reveal prevalent small agricultural fires ($<0.5 \times 10^4 \text{ m}^2$) in the extensive croplands that are not detected in the common satellite fires. As control measures get more stringent, spatial-temporal patterns as well as the scales of biomass burning activities in China have undergone dramatic changes. Considering the crucial role of satellite fires in estimating biomass burning emissions, it is necessary to improve satellite fire detection with more advanced observations and retrieval methods.

1. Introduction

Biomass burning is a global phenomenon that occurs in the vegetated terrestrial ecosystem. Every year, combustion of the open vegetation

fires emits large amounts of gases and aerosol particles into the atmosphere (Andreae et al., 2019; Langmann et al., 2009). Organic carbon and black carbon from biomass burning are estimated to account for about 62% and 27% of their global emissions (Wiedinmyer et al., 2011).

* Corresponding author. NO. 388, Lumo Road, Hongshan District, Wuhan, 430074, China.

E-mail address: taomh@cug.edu.cn (M. Tao).

<https://doi.org/10.1016/j.atmosenv.2021.118838>

Received 1 June 2021; Received in revised form 2 November 2021; Accepted 6 November 2021

Available online 9 November 2021

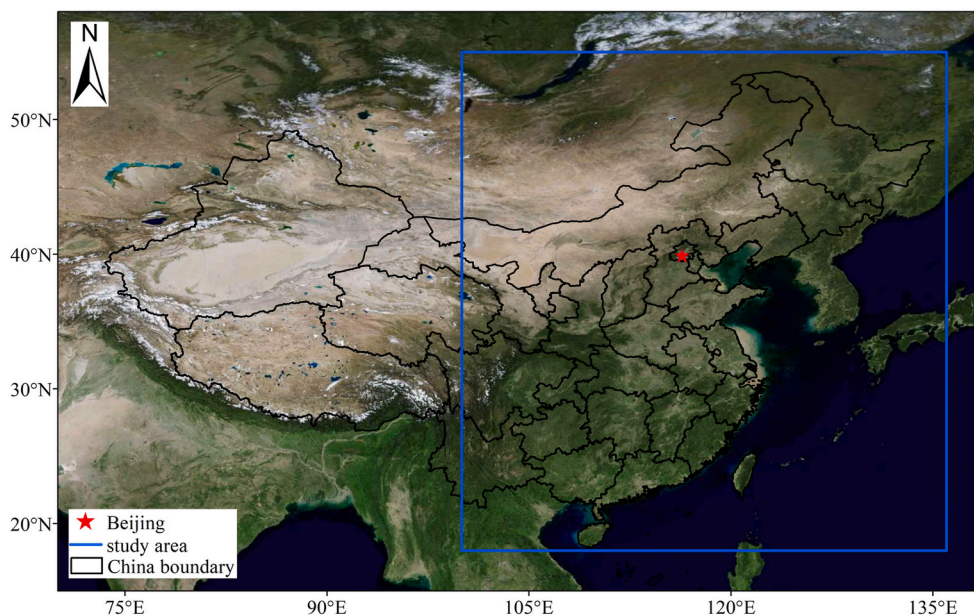


Fig. 1. Spatial extent (blue) of the study area (100–136°E, 18–55°N) in China.

Moreover, biomass burning emissions have important contributions to the increasing greenhouse gases including carbon dioxide (CO₂) and methane (CH₄) as well as other gaseous pollutants such as sulfur dioxide (SO₂) and nitrogen oxides (NO_x) (Streets et al., 2003). Therefore, emissions from biomass burning play a significant role in the environment and climate system (Chen et al., 2017; Crutzen and Andreae, 1990; Gupta et al., 2004; Koren et al., 2004), which are also the crucial inputs required by chemical transport and atmospheric circulation models (Pan et al., 2020).

Different from the concentrated pollution in urban/industrial areas, the large spatial and temporal variations of biomass burning fires pose a great challenge on their emission estimation and environment management. The abruptness and randomness of global vegetation fires as well as their varied burning areas make them hard to be effectively monitored by ground stations. As early as the 1980s, wide-swath satellite infrared observations with the advantage of daily global coverage have been used to identify active fires by detecting their intense thermal radiation (Dozier, 1981; Flannigan and Haar, 1986). Operational fire products from polar-orbiting satellite instruments such as Advanced Very High Resolution Radiometer (AVHRR) and Moderate Resolution Imaging Spectroradiometer (MODIS) have been developed (Giglio et al., 2003, 2009, 2016) and widely used (Wiedinmyer et al., 2011; Zhang et al., 2020). In particular, spatial and temporal resolutions of recent polar-orbiting and geostationary satellite instruments have been significantly improved (Li et al., 2020; Schroeder et al., 2014), allowing the detection of smaller, fast-burning fires.

Biomass burning in China has been shown to have widespread and complicated influences on regional air quality and climate (Chen et al., 2017). During the harvest season, dense agricultural straw burning fires exist in the vast croplands of eastern China (Tao et al., 2013). The intense emissions of these crop fires mix with local anthropogenic pollutants, and change optical properties of the aerosols (Li et al., 2010). With the favor of satellite fire detection, the Environment Protection Agency (EPA) of China has banned open burning of crop straws with daily satellite supervision (Wang et al., 2021). However, unlike the sustained bushfires with a large-scale burned area, the crop straw fires usually have a large spatial discreteness and a rapid burning process (Hall et al., 2016; Liu et al., 2019). By now, performance of the current satellite fire products in China remains unclear due to a lack of sufficient validations.

In this study, we present a comprehensive insight into performance

of the common satellite fire products with different spatial and temporal resolutions in eastern China during 2019. Also, accuracy of the operational fire products is validated by their inter-comparison as well as high-resolution satellite images at meter resolution. The fire detection algorithms of satellite products are introduced in section 2. General characteristics of the active fires from both polar-orbiting and geostationary satellites are compared in section 3.1. Then, performance of these satellite fire products is analyzed and discussed in section 3.2 and 3.3. Section 4 gives a brief summary of the conclusions.

2. Data and methods

2.1. Description of the study area

China is a major agricultural country of the world since ancient times. As shown in Fig. 1, most of the vegetation covers are concentrated in the broad plains of northeastern, northern, and central part of China, which is also the most populous regions of China. During the harvest season of every year, agricultural wastes such as crop straws from rice, wheat and maize are usually burned to clear the land quickly (Huang et al., 2012). Moreover, biomass burning fires exist in the mountains and hilly areas around the plains or in southern China. Considering that the western part of China is dominated by deserts and bare lands, we select the scope within 100–136°E, 25–50°N in eastern China as the study area.

2.2. Collection 6 MODIS fire product

By utilizing spectral brightness temperatures at 4 μm (T₄) and 11 μm (T₁₁) at 1 km, MODIS contextual algorithm can not only detect large high-temperature fires with absolute thresholds, but also identify smaller and cooler fires based on the statistical test of their differences with background non-fire pixels (Giglio et al., 2003, 2016). Also, confidence of the fire pixels is calculated depending on T₄ and the number of adjacent cloud and water pixels. Global validations of MODIS fire products by using coincident fire masks from 30 m satellite images show that omission error stabilizes at ~5% for MODIS pixels containing more than ~250 30 m fire pixels (Schroeder et al., 2008). Smaller fires with much smaller sizes can also be detected, but the omission fraction increases rapidly as the fire size. By contrast, the global commission error of MODIS fires is much lower at 1.2% (Giglio et al., 2016). We select the recent Collection (C) 6 MODIS fire products (MCD14ML) of all

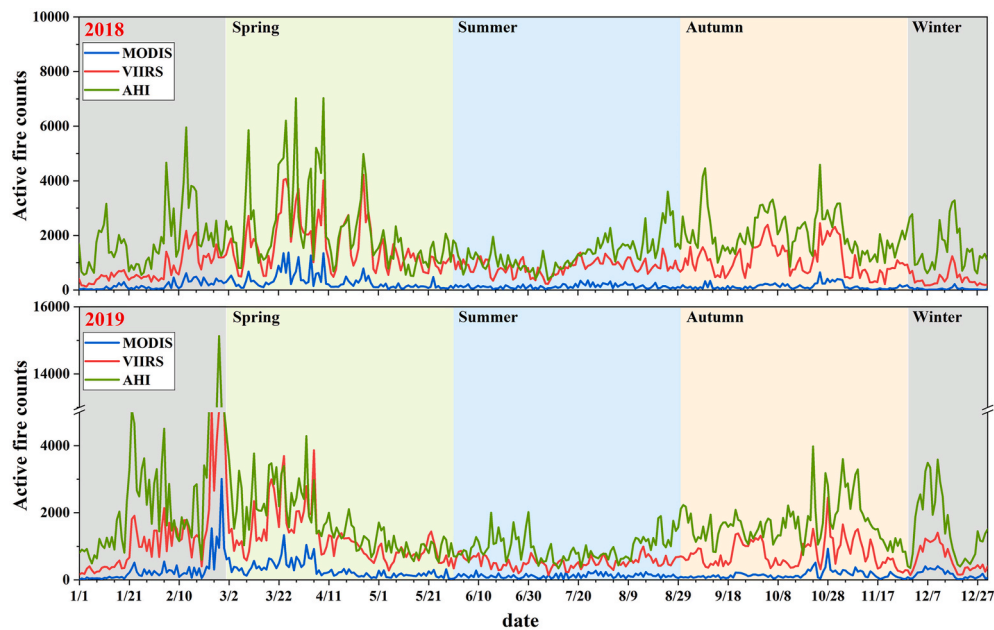


Fig. 2. Daily time series of fire counts in eastern China derived from MODIS (blue), VIIRS (red) and Himawari-8 AHI (green) during 2018 and 2019. (For interpretation of the references to color in this figure legend, the reader is referred to the Web version of this article.)

confidence from both the morning satellite Terra and afternoon Aqua for the analysis (<https://firms.modaps.eosdis.nasa.gov/>). Besides fire location, the rate of fire radiative energy (Joules per second or Watts), defined as Fire Radiative Power (FRP), is widely used as an indicator of fire emissions (Wooster and Zhang, 2004). MODIS Fire FRP is calculated as a function of $4 \mu\text{m}$ radiance and pixel size (Giglio et al., 2016).

2.3. Visible Infrared Imaging Radiometer Suite (VIIRS) fire product

As the successor of MODIS, VIIRS instrument is launched aboard the Suomi National Polar-orbiting Partnership (S-NPP) satellite in October 2011 and NOAA-20 satellite in November 2017, respectively. With higher spatial resolutions at 375 m and 750 m, VIIRS detection based on similar fire algorithm as MODIS can identify much smaller and cooler fires (Schroeder et al., 2014; Zhang et al., 2020). It should be stated that the time interval of NOAA-20 and S-NPP is around 50 min, and the VIIRS fires from NOAA-20 is available from 2020. To examine the influence of spatial resolution on fire detection, we utilize VIIRS 375 m fire products from the S-NPP satellite (VNP14IMG) for comparison (<https://firms.modaps.eosdis.nasa.gov/>).

2.4. Himawari-8 Advanced Himawari Imager (AHI) fire product

The next generation geostationary weather satellite, Himawari-8, was launched in October 2014 by the Japan Meteorological Agency (JMA). The Advanced Himawari Imager (AHI) onboard Himawari-8 measures spectral irradiance of the Earth-atmosphere system with 16 channels in $0.4\text{--}14 \mu\text{m}$ at a high temporal resolution of 10 min (Bessho et al., 2016; Zhang et al., 2019). Despite a spatial resolution of $0.5\text{--}1 \text{ km}$ in visible and near infrared bands, Himawari-8 has a relatively coarse pixel size of 2 km for middle and thermal infrared observations. Since Himawari-8 also has middle and thermal infrared bands as MODIS and VIIRS, contextual fire detection algorithm is utilized to detect the burning fires (Li et al., 2020). We select the 10-min Himawari-8 products to evaluate the influence of temporal resolution on fire detection (<ftp://ftp.ptree.jaxa.jp>). To avoid repetitive statistics of daily fire occurrence, we only count the Himawari-8 fires in the same location and the same day once.

2.5. PlanetScope and unmanned aerial vehicle (UAV) images

Most previous studies validate the satellite fires by 30 m Landsat images (Schroeder et al., 2008; Li et al., 2020), but it is difficult to obtain sufficient matchups in regional scales due to its long revisit circle of more than half a month. Also, these satellite images such as Landsat usually identify fires by burn-sensitive vegetation index rather than thermal radiation of the burning fire, which cannot reflect fire burning time. With a unique combination of spatial coverage in different orbits, PlanetScope constellation of approximately 200 satellites can obtain a daily image of the entire Earth at 3 m resolution. The PlanetScope sensor has four bands including blue, green, red and near infrared (<https://www.13harrisgeospatial.com/>), and fire burned area and burning in which day can be clearly identified in its RGB image. Moreover, the EPA in several provinces of China have utilized UAV images to monitor biomass burning in local scales (<http://sthjt.hubei.gov.cn/>). UAV observations with a high resolution at 0.1 m can easily detect very small fires of several square meters.

2.6. Validation

The different spatial and temporal resolutions of polar-orbiting and geostationary satellite fires make large-scale assessment of omission and commission errors with short-term data possible by their inter-comparison. Considering the difference of satellite fire products at spatial and temporal resolutions, fire numbers are calculated at unified grids and only counted once at one grid and one day. To have a detailed view of the performance of 375 m VIIRS fire products, we select PlanetScope and UAV RGB images in central China to make a validation at fine scales.

3. Results and discussions

3.1. Overall performance of satellite fires in China

To have a general view of the consistency and uncertainties of common satellite fires in eastern China, we first examine their spatial and temporal patterns. Fig. 2 shows time series of the active fire counts derived from 1 km MODIS, 375 m VIIRS and 2 km Himawari-8 AHI

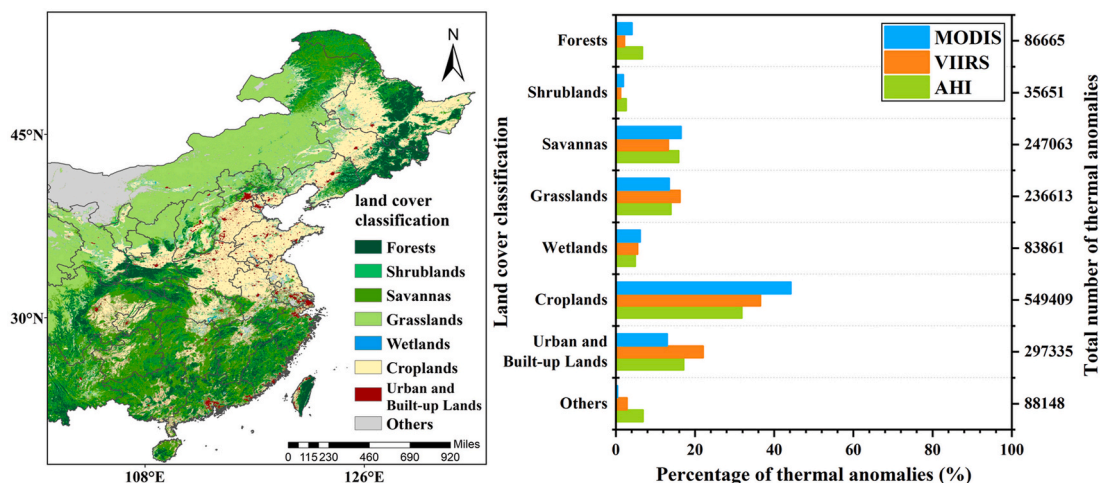


Fig. 3. Left) 500 m MODIS land cover types in eastern China, right) percentage of MODIS (blue), VIIRS (red), and Himawari-8 AHI (green) thermal anomalies over typical surface types during 2019. (For interpretation of the references to color in this figure legend, the reader is referred to the Web version of this article.)

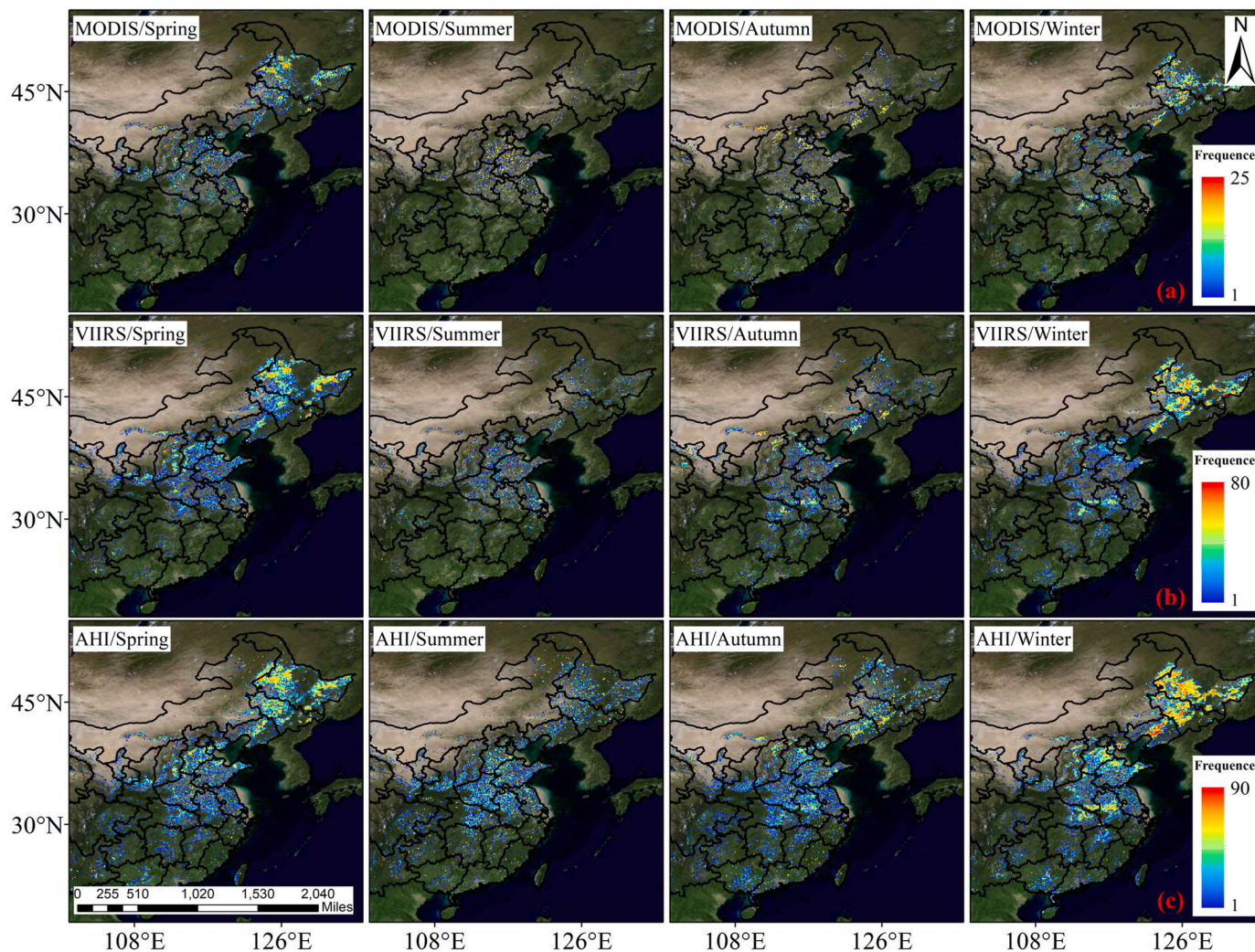


Fig. 4. Seasonal occurrence of 1 km MODIS (a), 375 m VIIRS (b) and 2 km Himawari-8 (c) fire counts in eastern China during 2019.

during 2018 and 2019 in eastern China (100–136°E, 25–50°N). Unlike the largest number of agricultural fires during summer around 2010 (Huang et al., 2012; Tao et al., 2013), the peaks of fire counts appear in spring, which are 2–3 times of those in summer and fall. The most

striking feature is the distinct discrepancy in fire numbers of different satellite products. Even fires in the same grid and the same day are counted only once, daily occurrence of the 10-min Himawari-8 fires is much higher than those from MODIS and VIIRS due to more fires

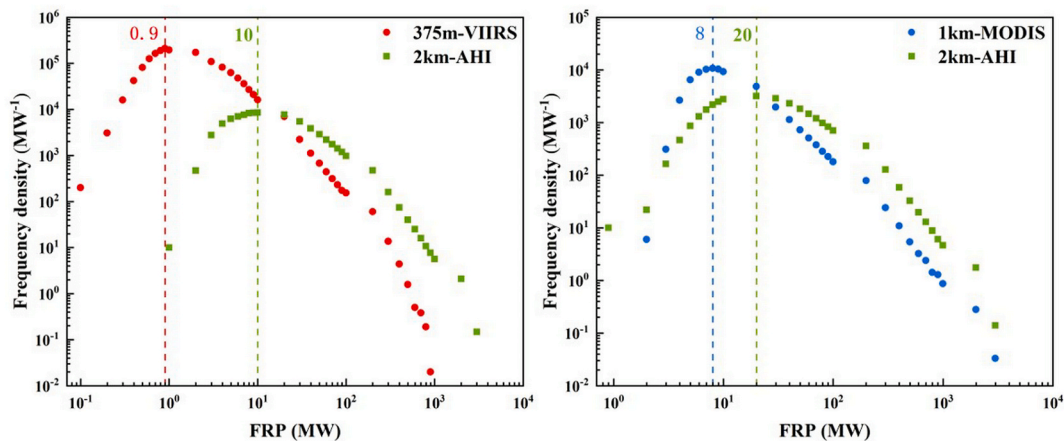


Fig. 5. Frequency density of 375 m VIIRS (left) and 1 km MODIS (right) fire FRP matched within 2 km Himawari-8 AHI FRP with a time window of ± 30 min of their overpass in eastern China during 2019.

detected by its high temporal resolution. Also, 375 m VIIRS fires have a much larger number than the 1 km MODIS and are close with Himawari-8's in spring. Although MODIS fires from both Terra and Aqua satellite are considered, their daily counts are very low (< 200) except in spring. As strict measures against agricultural fires implemented around 2010, the straw burning season switches from summer to spring, when the fire supervision can be less stringent within the non-harvest season.

The satellite fires in eastern China during 2019 are counted based on the C6 MODIS 500 m land cover product (MCD12Q1) (Fig. 3). MCD12Q1 divides global land covers into 17 categories with an overall accuracy of 73.6% (Sulla-Menashe et al., 2019). Some smaller categories in MCD12Q1 are merged and there are 8 surface types utilized in eastern China. Fires in croplands account for the largest percentage of approximately 40%, and those in savannas and grasslands contribute to $\sim 15\%$ of the total thermal anomalies, respectively. It is worth noting that $\sim 15\text{--}20\%$ of the thermal anomalies appear in urban/industrial regions, which can be caused by the intense industrial heat emissions (Li et al., 2021). Considering that the lack of croplands in the 500 m MODIS land covers is not reasonable in several provinces of southern part, many agricultural fires in the fragmented croplands can be classified into savannas. Additionally, fire counts in the wetlands and forests are at a much lower level in eastern China with a percentage of $\sim 6\%$ and $\sim 2\text{--}4\%$, respectively.

To have a direct view of spatial patterns of the fires, their seasonal frequency in eastern China during 2019 is shown in Fig. 4. Compared with the fire occurrence around 2010 (Huang et al., 2012; Tao et al., 2013), spatial distribution of the biomass burning exhibits a dramatic transition. The intense agricultural fires in the Northern China Plain (NCP) in summer have nearly disappeared during 2019. Moreover, biomass burning hotspots move from NCP in summer to northeastern China in spring and winter, which can be largely caused by diverse control measures of crop straw burning in difference provinces. The biomass burning hotspots in the NCP and southern China are very scattered.

Despite consistent spatial patterns, seasonal occurrence of MODIS, VIIRS and Himawari-8 fires have distinct magnitudes (Fig. 4). The spatial occurrence of VIIRS fires is 2–3 times of MODIS's due to much more fires detected by the high spatial resolution. By contrast, spatial occurrence of Himawari-8 fires is much larger than MODIS and VIIRS ones, implying that many fires with rapid burning process have been missed by the polar-orbiting observations. Although Himawari-8 observes fires over most vegetated regions in eastern China, their low frequency except in northeastern China demonstrates that the used large-scale agricultural straw burning has been effectively controlled (Huang et al., 2012). On the other hand, the much fewer 1 km MODIS fires than 375 m VIIRS indicates that 2 km Himawari-8 detection can

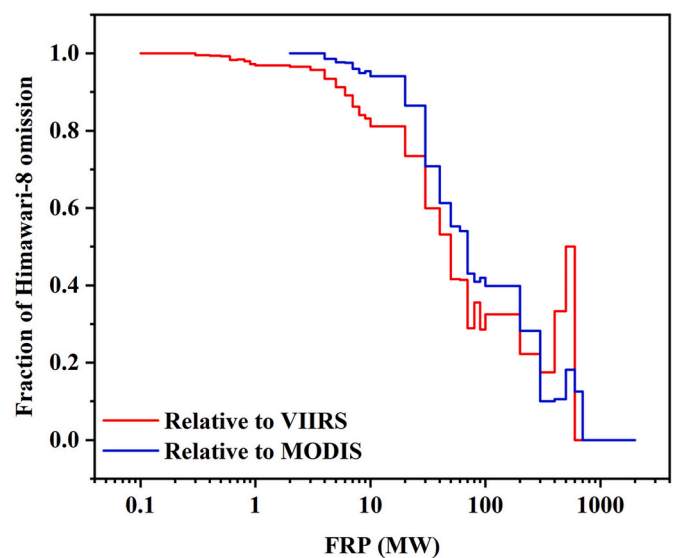


Fig. 6. Himawari-8 fire omission fraction in the total matchups with 375 m VIIRS (red) and 1 km MODIS (blue) fire counts and its variations with VIIRS and MODIS FRPs. (For interpretation of the references to color in this figure legend, the reader is referred to the Web version of this article.)

omit a large number of VIIRS and MODIS fires.

3.2. Omission error of satellite fires estimated by their inter-comparison

Fig. 5 shows frequency density of VIIRS and MODIS FRP values matched with 2 km Himawari-8 fires within ± 30 min of their overpass respectively during 2019. While the upper detection limit of Himawari-8 FRP ($\sim 10^5$ MW) is much higher than VIIRS's ($\sim 10^3$ MW), the lower detection limit of VIIRS (~ 0.1 MW) is obviously lower than that of Himawari-8 (~ 1 MW). Compared with the 2 km Himawari-8, 375-m VIIRS is very sensitive to low-FRP fires, but can be saturated at high temperatures. In particular, VIIRS FRP values are most frequent at 0.9 MW, which can be dominated by the small-area agricultural straw burning fires. By contrast, both MODIS and Himawari-8 can hardly detect low-FRP fires (< 1 MW) such as the scattered agricultural burning. Although distribution range of MODIS FRP values is similar as that of Himawari-8's, 1-km MODIS can detect more low-FRP values (< 20 MW).

To quantify the performance of Himawari-8 products in eastern China, we calculate the omission fraction of Himawari-8 fire detection compared with contemporaneous 375 m VIIRS and 1 km MODIS

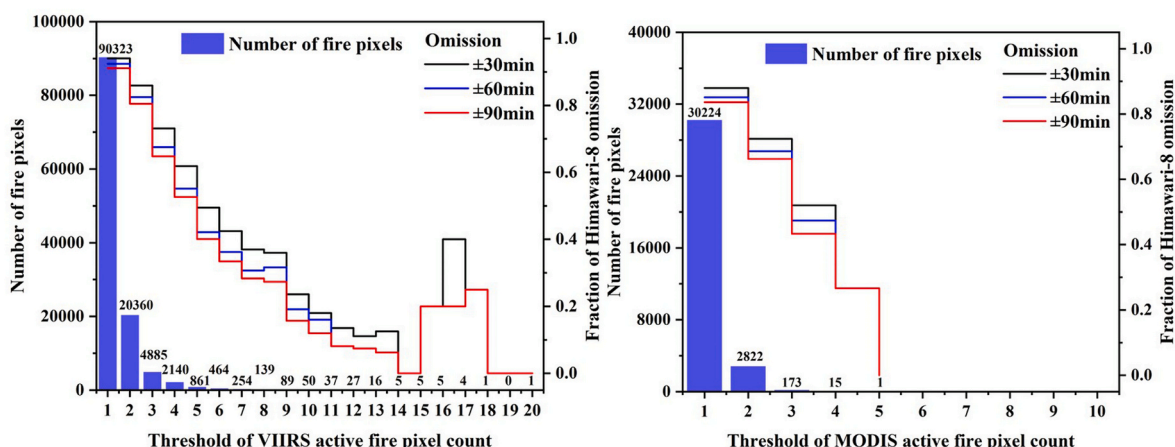


Fig. 7. Number and omission fraction of 2 km Himawari-8 fires matched up with left) 375 m VIIRS and right) 1 km MODIS fire pixels in different time windows.

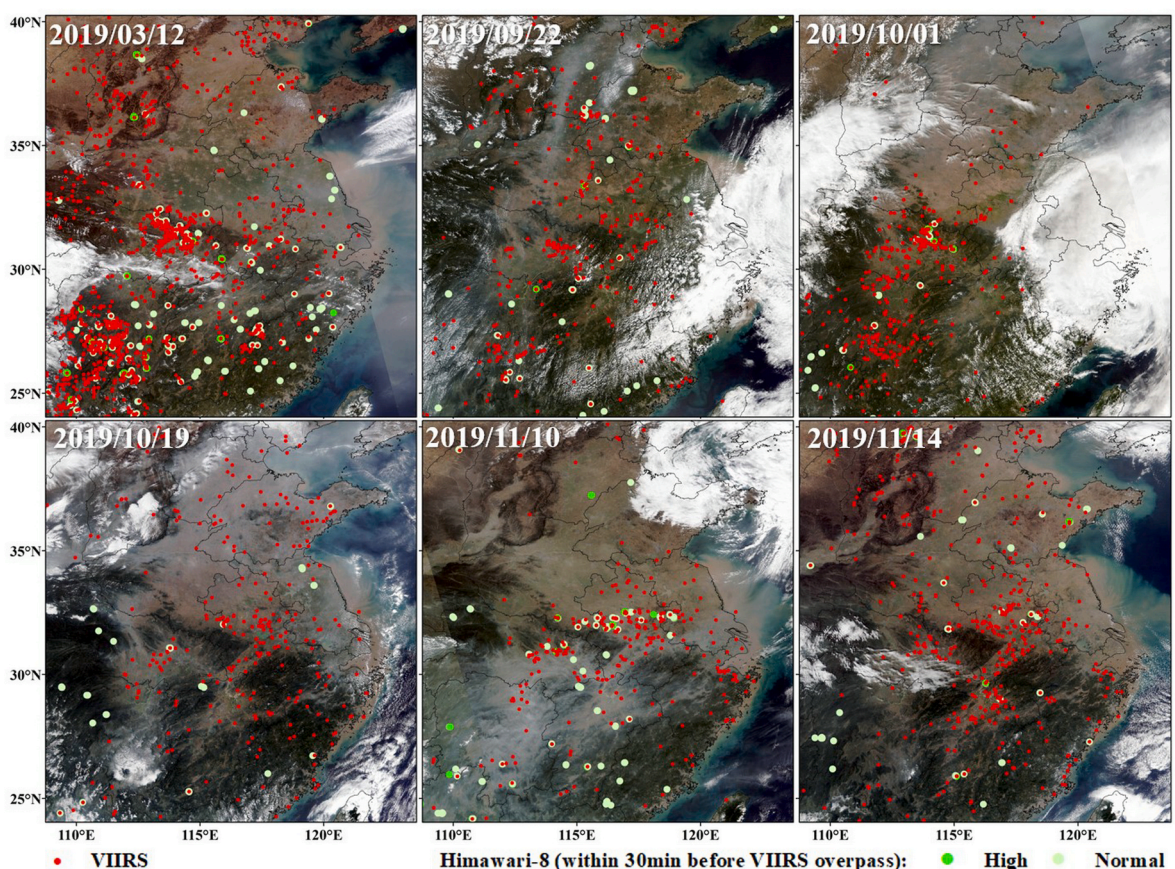


Fig. 8. Comparison of 375 m VIIRS (red) of all confidence and 2 km Himawari-8 fires (green) within 30 min before VIIRS's overpass. (For interpretation of the references to color in this figure legend, the reader is referred to the Web version of this article.)

observations of different FRPs (Fig. 6). It can be seen that omission error of Himawari-8 fire detection is nearly 100% when VIIRS FRP is smaller than ~2 MW. Moreover, the lack of MODIS FRP in this range demonstrates that ~2 MW is the lower detection limit of MODIS. When VIIRS and MODIS FRP increases from 10 MW to 300 MW, the omission error of Himawari-8 fire detection declines from ~80% to ~20%. There is a sudden increase in the omission error of Himawari-8 detection at high-FRP (~400–900 MW) of matched VIIRS fires (Fig. 6), indicating that the dense smoke of biomass burning can hamper fire detection (Csiszar et al., 2006). It should be stated that stagnant or moist weather conditions as well as burning state such as smoldering fires can also favor the

generation of heavy smoke.

Fig. 7 displays the histograms of 375 m VIIRS fires within the 2 km Himawari-8 pixel counting by the number of contemporaneous VIIRS fire pixels. Meanwhile, omission error of Himawari-8 fires is examined by comparing with VIIRS and MODIS products in different time windows. Even in a spatial extent of a 2 × 2 km, single-pixel 375 m VIIRS fires are predominant with a total number of 90323 in eastern China during 2019. Then, the frequency of multi-pixel 375 m VIIRS fires declines exponentially as the number of VIIRS fire pixels within the Himawari-8 pixel increases. Similar as that in Fig. 6, the omission error of Himawari-8 detection decreases consistently within more VIIRS fires

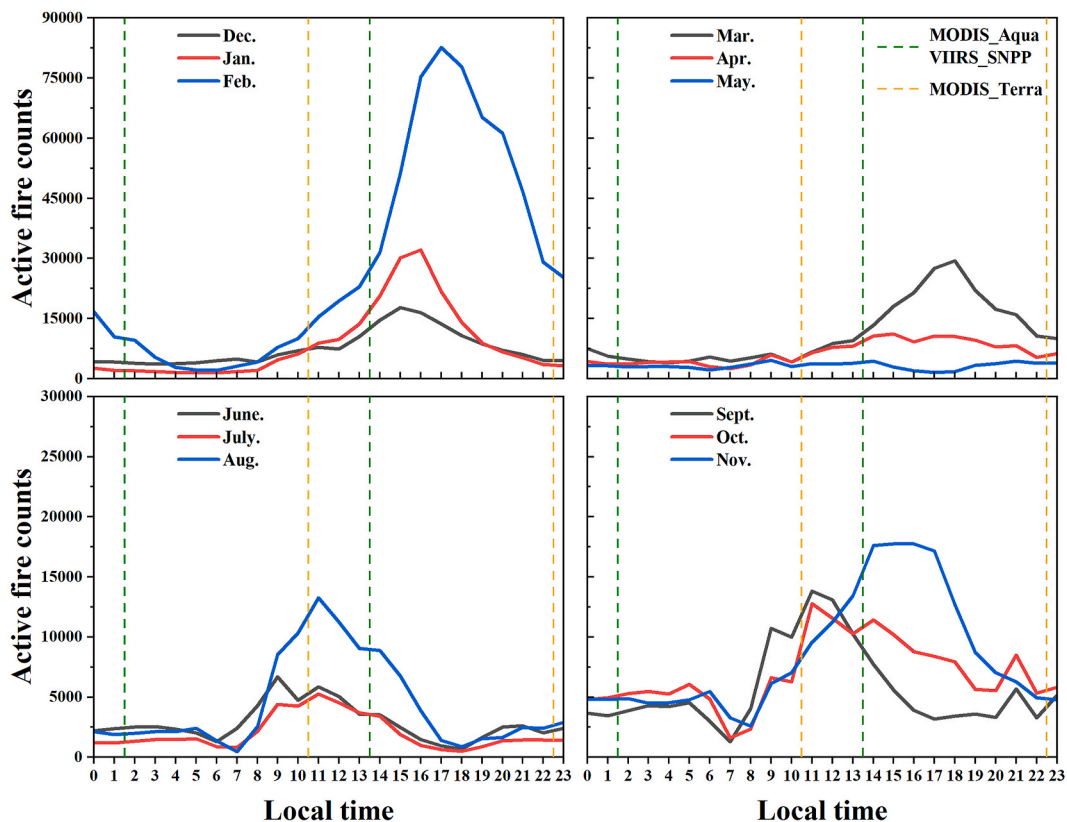


Fig. 9. Diurnal variations of Himawari-8 fire counts of different seasons in eastern China during 2019. The dashed lines denote passing time of MODIS and VIIRS.

in its pixel, meaning higher FRP from large fire areas. Despite consistent performance, the number of 1-km MODIS fires is no more than one third of VIIRS's. With the strict control measures, the agricultural burning in eastern China is dominated by scattered low-FRP and small-area fires.

As the temporal windows of Himawari-8 detection compared with matched VIIRS and MODIS fires increases from 30 min to 90 min, its omission error decreases by ~10% due to detection of emerging fires or maximum FRP of the burning (Fig. 7). Although Himawari-8 detection misses most of the VIIRS and MODIS fires, its much higher fire frequency in seasonal scales in the overall eastern China demonstrates that temporal resolution of the polar-orbiting VIIRS and MODIS observations is far from enough to capture most of the biomass burning fires in eastern China (Fig. 4). It is surprising that the lowest omission errors of Himawari-8 fires keep at ~10% rather than close to 0 with more than 10 VIIRS fire pixels in. Compared with the 375-m VIIRS observations, the 2 km Himawari-8 detection can be more likely obscured by the dense fire

smoke (Csiszar et al., 2006).

3.3. Uncertainties of satellite fire detection in China

Owing to the coarse spatial resolution of Himawari-8 observations, it is expected that the detected fires by Himawari-8 are strong enough to be detected by VIIRS and MODIS. However, comparison of concurrent fire images shows that even 375-m VIIRS detection cannot identify some of the Himawari-8 fires (Fig. 8), demonstrating that the current Himawari-8 algorithm can introduce false fires at both high and low confidence. Similar algorithm flaws also exist in the Geostationary Operational Environmental Satellite (GOES)-16 fires in North America (Li et al., 2020). For the 2 km coarse resolution, threshold training of satellite fire algorithms can be difficult in striking a balance between the number of detectable fires and detection accuracy, especially for the small agricultural fires. Considering that the 10-min Himawari-8

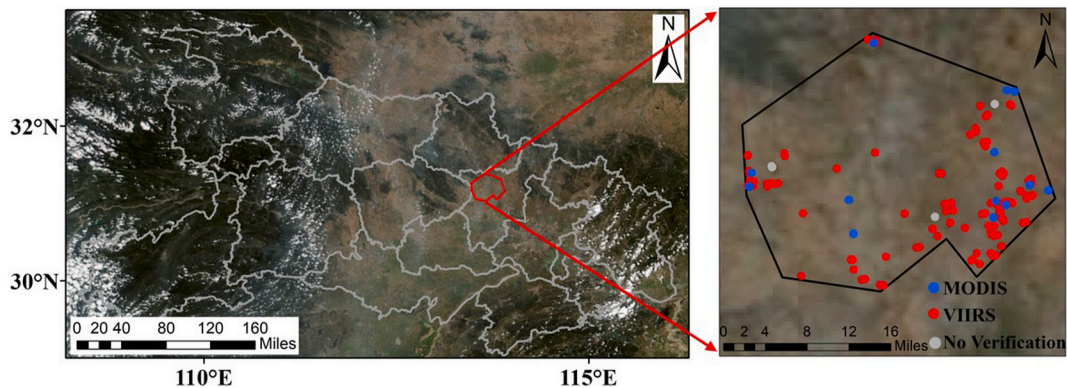


Fig. 10. Validation area is located within Xiaogan City of Hubei province, and the time of VIIRS (red) and MODIS (blue) fires are from Sept. 1 to Oct. 8, 2019. (For interpretation of the references to color in this figure legend, the reader is referred to the Web version of this article.)

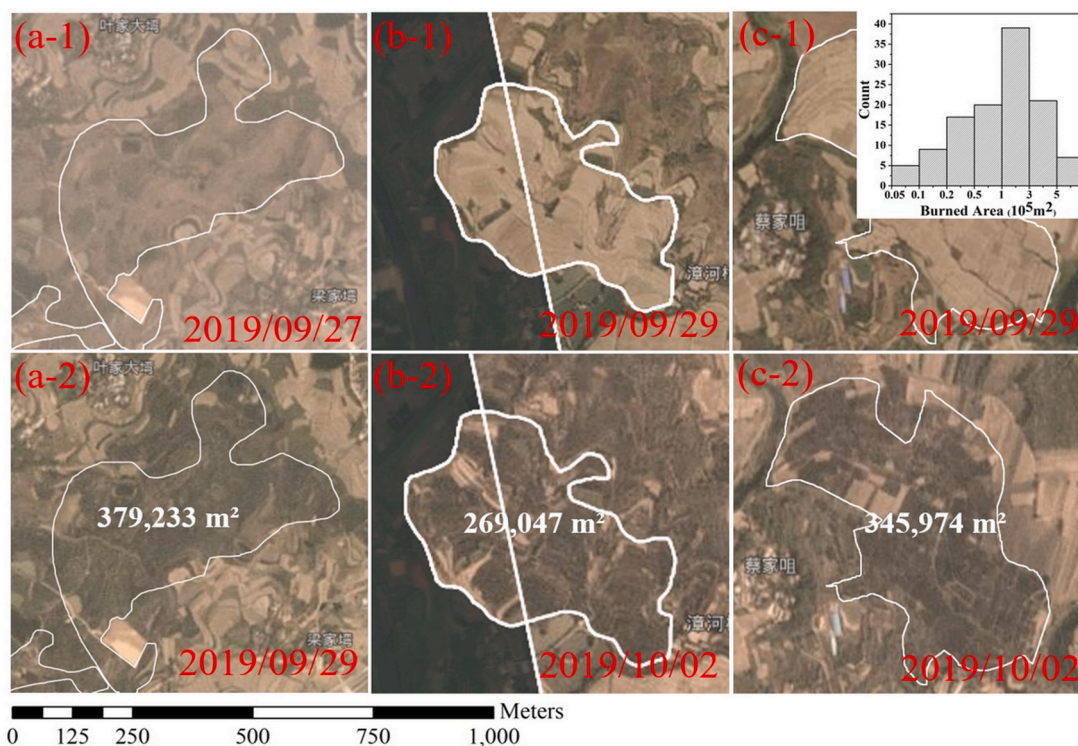


Fig. 11. PlanetScope true color images before and after three fire events in central China. The histogram in the top right corner is the burned areas of the 104 VIIRS fires found in PlanetScope images. (For interpretation of the references to color in this figure legend, the reader is referred to the Web version of this article.)

Table 1
The commission errors of VIIRS and MODIS comparison of high-resolution.

| VIIRS | PS Images | Fire points | Commission error |
|-------|------------------------|-------------|-------------------|
| | 61 | 108 | 3.7% |
| | Counts detected by AHI | | Relative omission |
| | 3 | | 97.2% |
| MODIS | PS Images | Fire points | Commission error |
| | 12 | 13 | 0.0% |
| | Counts detected by AHI | | Relative omission |
| | 0 | | 100.0% |

detection can provide indispensable information regarding diurnal cycles of the biomass burning, it is necessary to adopt more stringent thresholds or methods to ensure a higher accuracy of the fire products.

Diurnal variations of the biomass burning activities can be a crucial factor in influencing polar-orbiting satellite fire detection. As shown in Fig. 9, the monthly fire counts in eastern China exhibit distinct temporal patterns in different seasons. The biomass burning in eastern China is concentrated in the afternoon during winter and spring, and fire counts peak around 16:00 at local time and even later. VIIRS and MODIS flying over eastern China around 13:30 cannot detect the numerous fires emerging after their overpass. By contrast, the peaks of the fires move up

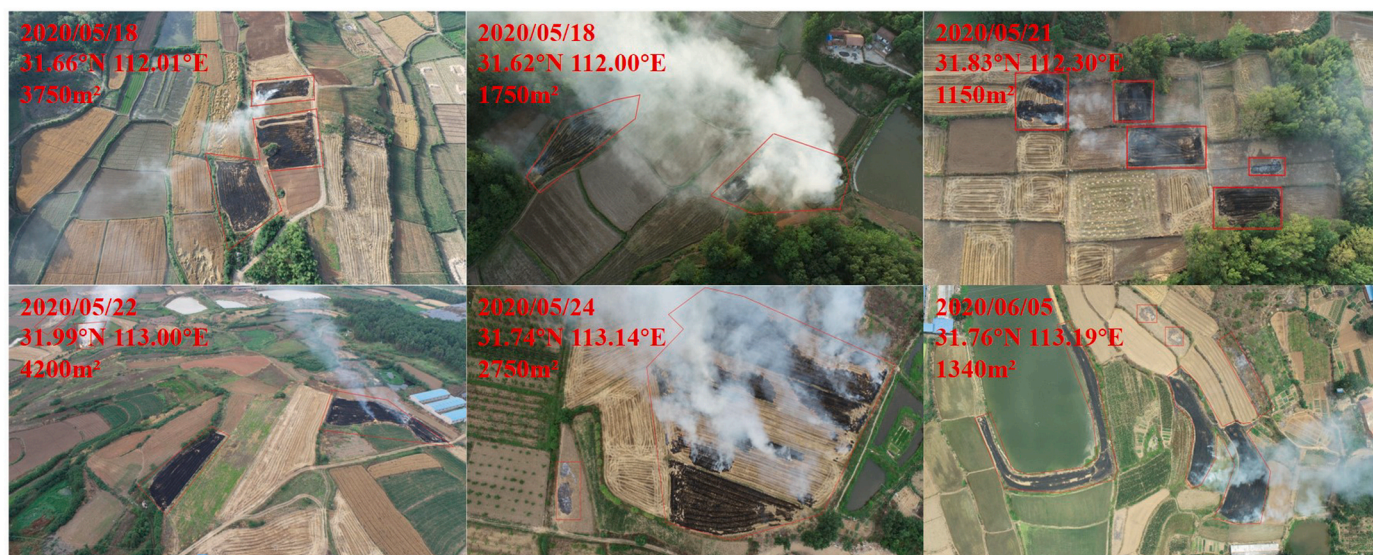


Fig. 12. UAV true color images of the crop fire events and their burned area in central China. (For interpretation of the references to color in this figure legend, the reader is referred to the Web version of this article.)

to the noon in summer and fall. Time shift of the biomass burning activities can be caused by changing weather conditions and harvest habits in different seasons. Furthermore, the peak time of the biomass burning dominated by agricultural straw fires is usually within ~1–3 h, due mostly like to the rapid burning process of the cropland fires.

To evaluate the absolute accuracy of satellite fires, we utilize PlanetScope images in a typical agricultural area of central China before and after VIIRS (red) and MODIS (blue) fires to confirm whether biomass burning exist (Fig. 10). A total of 108 375 m VIIRS (red) and 13 1 km MODIS (blue) thermal anomaly pixels is detected within the selected area. As shown in Fig. 11, the visual transition from unburned, dry croplands (yellow) to burned (black) is visible in the satellite RGB images after burning. Except that four VIIRS thermal anomaly pixels cannot be confirmed due to a lack of matching high-resolution satellite images, all the remaining VIIRS and MODIS fires are proved to be correct (Table 1). However, Himawari-8 misses all the MODIS fires, and only three fire pixels are matched with VIIRS results. Despite limited samples, the validation shows that VIIRS and MODIS fires have a very high accuracy. However, many of the scattered and small agricultural fires can be out of the lower detection limit of even 375 m VIIRS (Hall et al., 2021).

The agricultural fires detected by 375 m VIIRS observations tend to have a burned area exceeding 10^4 m^2 , which is approximately one-tenth (~7%) of VIIRS pixel size (Fig. 11). Unlike the fierce forest fires with high temperatures, achieving the lower detection limit (~0.1 MW) of even 375 m VIIRS requires the crop straw burning has large enough areas (Fig. 5). We also validate VIIRS fires with the UAV RGB images in central China. Although numerous fires are found by UAV images (Fig. 12), very few of them has been matched with VIIRS fires. The burned areas in the UAV images are usually below $0.5 \times 10^4 \text{ m}^2$, and even around 100 m^2 , which is much smaller than the fire areas of agricultural burning VIIRS can detect. The strict supervision measures have greatly eliminated concentrated agricultural fires, but biomass burning for cleaning the straw wastes are still prevalent at much smaller scales. These abundant small fires in the extensive croplands can account for a substantial fraction in the total emissions of the biomass burning, which has also been largely underestimated in other regions of the world (Hall et al., 2021). Since spatial coverage of the UAV observations is confined to local scales, how to quantify emissions of these small fires in the biomass burning inventory is a challenge.

The combination of polar-orbiting and geostationary satellite observations can enhance fire detection in eastern China. Zhang et al. (2020) improves the underestimation of biomass burning emissions in eastern China by using spatial patterns of VIIRS fires and the diurnal cycles of Himawari-8 FRP. However, accurate estimation of the biomass burning emissions in China can be hindered by several considerable uncertainties (Wang et al., 2018). Considering that the small agricultural fires in eastern China usually have much smaller areas than satellite pixel such as 375 m VIIRS and 1 km MODIS, information of the actual burned area or FRP is crucial in their emission estimation (Peterson et al., 2013; Wooster et al., 2003). The croplands in China are characterized by separated small fields with clear boundaries, so the agricultural burning usually occurs in fixed areas rather than spread around. Also, whether diurnal cycles of Himawari-8 fire counts and FRP can represent characteristics of the prevalent small fires needs more examinations. In particular, biomass burning in eastern China is going through dramatic changes due to both more stringent control measures and rapidly developing agricultural activities. Additionally, the abundant small fires cannot be detected by the current satellite products should be considered with improved algorithms as well as high-resolution observations such as PlanetScope and UAV images.

4. Conclusions

The massive emission of biomass burning play a significant role in air quality and climate change. Although satellite fire products have

provided fundamental constraints for estimation of global biomass burning emissions, their limitations in spatial and temporal scales can lead to high-level uncertainties in both satellite fire detection and emission estimation. In this study, we present an overview of the performance of common satellite fire products in eastern China. Owing to the limitation in spatial and temporal resolutions, both polar-orbiting and geostationary satellite observations have large omission ratios in detecting the abundant agricultural fires with small areas and rapid burning process. The inter-comparison between concurrent 375 m VIIRS and 2 km Himawari-8 products shows that Himawari-8 detection misses nearly 90% of the VIIRS fires. By contrast, the whole amount of daily VIIRS and MODIS fires in eastern China is only less than one-half and one-quarter of Himawari-8 results because many fires out of their passing time cannot be detected.

Even at all confidence, VIIRS and MODIS fire detections have very high accuracy in the validation with high-resolution satellite images. However, Himawari-8 fires have important algorithm flaws with notable false alarms. Moreover, the 2 km Himawari-8 detection is more likely to be influenced by dense smoke with an omission ratio of ~10% even when the FRP or burned area are relatively large. UAV observations reveal numerous agricultural fires with burned areas below $0.5 \times 10^4 \text{ m}^2$ in the croplands of eastern China, which cannot be detected by the common satellite products. With more stringent control measures, the biomass burning in China has undergone dramatic changes with smaller scales but frequent occurrence. To improve estimation of biomass burning emissions, more advanced observations and retrieval methods are in need.

CRedit authorship contribution statement

Jinxi Chen: Conceptualization, Writing – original draft. **Rong Li:** Methodology, Visualization. **Minghui Tao:** Writing – review & editing. **Lili Wang:** Investigation. **Changqing Lin:** Investigation. **Jun Wang:** Resources. **Lunche Wang:** Resources. **Yi Wang:** Investigation. **Liangfu Chen:** Supervision.

Declaration of competing interest

The authors declare that they have no known competing financial interests or personal relationships that could have appeared to influence the work reported in this paper.

Acknowledgments

This study was supported by National Natural Science Foundation of China (Grant No. 42171354 and 41830109) and Strategic Priority Research Program of the Chinese Academy of Sciences (Grant No. XDA19040201). Jun Wang's participation is made possible via the in-kind support from the University of Iowa. We thank the VIIRS, MODIS, Himawari-8 fire team for the data used in our work.

References

- Andreae, M.O., 2019. Emission of trace gases and aerosols from biomass burning – an updated assessment. *Atmos. Chem. Phys.* 19 (13), 8523–8546.
- Bessho, K., Date, K., Hayashi, M., Ikeda, A., Imai, T., Inoue, H., et al., 2016. An introduction to Himawari-8/9—Japan's new-generation geostationary meteorological satellites. *J. Meteorol. Soc. Japan. Ser. II* 94 (2), 151–183.
- Chen, J., et al., 2017. A review of biomass burning: emissions and impacts on air quality, health and climate in China. *Sci. Total Environ.* 579, 1000–1034.
- Crutzen, P.J., Andreae, M.O., 1990. Biomass burning in the tropics: impact on atmospheric chemistry and biogeochemical cycles. *Science* 250 (4988), 1669–1678.
- Csiszar, I.A., Morisette, J.T., Giglio, L., 2006. Validation of active fire detection from moderate-resolution satellite sensors: the MODIS example in northern Eurasia. *IEEE Trans. Geosci. Rem. Sens.* 44 (7), 1757–1764.
- Dozier, J., 1981. A method for satellite identification of surface temperature fields of subpixel resolution. *Rem. Sens. Environ.* 11, 221–229. [https://doi.org/10.1016/0034-4257\(81\)90021-3](https://doi.org/10.1016/0034-4257(81)90021-3).
- Flannigan, M.D., Haar, T.H.V., 1986. Forest fire monitoring using NOAA satellite AVHRR. *Canadian. J. For. Res.* 16 (5), 975–982.

- Giglio, L., Descloitres, J., Justice, C.O., Kaufman, Y.J., 2003. An enhanced contextual fire detection algorithm for MODIS. *Rem. Sens. Environ.* 87 (2–3), 273–282. [https://doi.org/10.1016/s0034-4257\(03\)00184-6](https://doi.org/10.1016/s0034-4257(03)00184-6).
- Giglio, L., Schroeder, W., Justice, C.O., 2016. The collection 6 MODIS active fire detection algorithm and fire products. *Rem. Sens. Environ.* 178, 31–41. <https://doi.org/10.1016/j.rse.2016.02.054>.
- Giglio, L., Loboda, T., Roy, D.P., Quayle, B., Justice, C.O., 2009. An active-fire based burned area mapping algorithm for the MODIS sensor. *Rem. Sens. Environ.* 113 (2), 408–420.
- Gupta, P.K., Sahai, S., Singh, N., Dixit, C.K., Singh, D.P., Sharma, C., Tiwari, M.K., Gupta, R., Garg, S.C., 2004. Residue burning in rice–wheat cropping system: causes and implications. *Curr. Sci.* 1713–1717.
- Hall, J.V., Loboda, T.V., Giglio, L., McCarty, G.W., 2016. A MODIS-based burned area assessment for Russian croplands: mapping requirements and challenges. *Rem. Sens. Environ.* 184, 506–521.
- Hall, J.V., Zibtsev, S.V., Giglio, L., Skakun, S., Myroniuk, V., Zhuravel, O., et al., 2021. Environmental and political implications of underestimated cropland burning in Ukraine. *Environ. Res. Lett.* 16 (6), 064019.
- Huang, X., Li, M., Li, J., Song, Y., 2012. A high-resolution emission inventory of crop burning in fields in China based on MODIS Thermal Anomalies/Fire products. *Atmos. Environ.* 50, 9–15, 0.
- Koren, I., Kaufman, Y.J., Remer, L.A., Martins, J.V., 2004. Measurement of the effect of amazon smoke on inhibition of cloud formation. *Science* 303 (5662), 1342–1345.
- Langmann, B., Duncan, B., Textor, C., Trentmann, J., van der Werf, G.R., 2009. Vegetation fire emissions and their impact on air pollution and climate. *Atmos. Environ.* 43 (1), 107–116. <https://doi.org/10.1016/j.atmosenv.2008.09.047>.
- Li, F., Zhang, X., Kondragunta, S., Schmidt, C.C., Holmes, C.D., 2020. A preliminary evaluation of GOES-16 active fire product using Landsat-8 and VIIRS active fire data, and ground-based prescribed fire records. *Rem. Sens. Environ.* 237, 111600. <https://doi.org/10.1016/j.rse.2019.111600>.
- Li, R., Tao, M., Zhang, M., Chen, L., Wang, L., Wang, Y., et al., 2021. Application potential of satellite thermal anomaly products in updating industrial emission inventory of China. *Geophys. Res. Lett.* 48, e2021GL092997 <https://doi.org/10.1029/2021GL092997>.
- Li, W.J., Shao, L.Y., Buseck, P.R., 2010. Haze types in Beijing and the influence of agricultural biomass burning. *Atmos. Chem. Phys.* 10 (17), 8119–8130.
- Liu, T., Marlier, M.E., Karambelas, A., Jain, M., Singh, S., Singh, M.K., DeFries, R.S., 2019. Missing emissions from post-monsoon agricultural fires in northwestern India: regional limitations of MODIS burned area and active fire products. *Environ. Res. Commun.* 1 (1), 011007.
- Pan, X., et al., 2020. Six global biomass burning emission datasets: intercomparison and application in one global aerosol model. *Atmos. Chem. Phys.* 20 (2), 969–994.
- Peterson, D., Wang, J., Ichoku, C., Hyer, E., Ambrosia, V., 2013. A sub-pixel-based calculation of fire radiative power from MODIS observations: 1: algorithm development and initial assessment. *Rem. Sens. Environ.* 129, 262–279.
- Schroeder, W., Prins, E., Giglio, L., Csiszar, I., Schmidt, C., Morisette, J., Morton, D., 2008. Validation of GOES and MODIS active fire detection products using ASTER and ETM+ data. *Rem. Sens. Environ.* 112 (5), 2711–2726. <https://doi.org/10.1016/j.rse.2008.01.005>.
- Schroeder, W., Oliva, P., Giglio, L., Csiszar, I.A., 2014. The New VIIRS 375m active fire detection data product: algorithm description and initial assessment. *Rem. Sens. Environ.* 143, 85–96. <https://doi.org/10.1016/j.rse.2013.12.008>.
- Streets, D.G., Yarber, K.F., Woo, J.H., Carmichael, G.R., 2003. Biomass burning in Asia: annual and seasonal estimates and atmospheric emissions. *Global Biogeochem. Cycles* 17 (4).
- Sulla-Menashe, D., Gray, J.M., Abercrombie, S.P., Friedl, M.A., 2019. Hierarchical mapping of annual global land cover 2001 to present: the MODIS Collection 6 Land Cover product. *Rem. Sens. Environ.* 222, 183–194. <https://doi.org/10.1016/j.rse.2018.12.013>.
- Tao, M., Chen, L., Wang, Z., Tao, J., Su, L., 2013. Satellite observation of abnormal yellow haze clouds over East China during summer agricultural burning season. *Atmos. Environ.* 79, 632–640, 0.
- Wang, J., Yue, Y., Wang, Y., Ichoku, C., Ellison, L., Zeng, J., 2018. Mitigating satellite-based fire sampling limitations in deriving biomass burning emission rates: application to WRF-chem model over the northern sub-Saharan African region. *J. Geophys. Res.: Atmosphere* 123 (1), 507–528.
- Wang, Z., et al., 2021. Systematics of atmospheric environment monitoring in China via satellite remote sensing. *Air Qual. Atmos. Health* 14 (2), 157–169.
- Wiedinmyer, C., Akagi, S.K., Yokelson, R.J., Emmons, L.K., Al-Saadi, J.A., Orlando, J.J., Soja, A.J., 2011. The Fire Inventory from NCAR (FINN): a high resolution global model to estimate the emissions from open burning. *Geosci. Model Dev. (GMD)* 4, 625–641. <https://doi.org/10.5194/gmd-4-625-2011>.
- Wooster, M.J., Zhukov, B., Oertel, D., 2003. Fire radiative energy for quantitative study of biomass burning: derivation from the BIRD experimental satellite and comparison to MODIS fire products. *Rem. Sens. Environ.* 86 (1), 83–107. [https://doi.org/10.1016/s0034-4257\(03\)00070-1](https://doi.org/10.1016/s0034-4257(03)00070-1).
- Wooster, M.J., Zhang, Y.H., 2004. Boreal forest fires burn less intensely in Russia than in North America. *Geophys. Res. Lett.* 31 (20).
- Zhang, Z., Fan, M., Wu, W., Wang, Z., Tao, M., Wei, J., Wang, Q., 2019. A simplified aerosol retrieval algorithm for Himawari-8 advanced Himawari imager over Beijing. *Atmos. Environ.* 199, 127–135.
- Zhang, T., de Jong, M.C., Wooster, M.J., Xu, W., Wang, L., 2020. Trends in eastern China agricultural fire emissions derived from a combination of geostationary (Himawari) and polar (VIIRS) orbiter fire radiative power products. *Atmos. Chem. Phys.* 20 (17), 10687–10705.